Journal of Materials Processing Technology 231 (2016) 58–65

Contents lists available at ScienceDirect

Journal of Materials Processing Technology

journal homepage: www.elsevier.com/locate/jmatprotec

Laser welding of CP Ti to stainless steel with different temporal pulse shapes

Hui-Chi Chen*, Guijun Bi, Bing Yang Lee, Chek Kweng Cheng

Singapore Institute of Manufacturing Technology, 71 Nanyang Drive, Singapore 638075

ARTICLE INFO

Article history:
Received 30 July 2015
Received in revised form 8 December 2015
Accepted 17 December 2015
Available online 23 December 2015

Keywords:
Laser welding
Dissimilar materials
Titanium
Stainless steel
Pulse profile

ABSTRACT

CP Ti and stainless steel sheets were laser welded by using a pulsed wave Nd:YAG laser welding system. The effect of pulse profiles used in laser welding was studied by investigating weld appearance, weld geometry, microstructure, hardness variation, joint strength and failure mode of welds. Weld quality was strongly affected by the temporal pulse profile adopted in laser welding. In comparison with the use of a normal rectangular pulse profile, stronger welds with a better homogeneity and a complex fracture mode were achieved by using a ramp-down pulse profile. This quality enhancement was contributed from the less degree of intermixing between two welding materials in melting pools.

1. Introduction

Welding of dissimilar materials is continuously attracting attention by the industry because of its potential benefits on saving material cost, reducing weight, increasing design flexibility and complexity as well as enhancing product functionality. Some unsolved issues remain in the process, in particularly, the degradation of mechanical properties which mainly results from the formation of brittle intermetallic phases in welds. Meco et al. (2015) indicated the joint strength was determined by the amount of intermetallic phases in joining of structure steel to Al alloy, while Chen et al. (2011a) found intermetallic phases were effectively reduced in laser welding of Zn-coated steel to Al alloy by using nitrogen shielding gas. In laser welding of Li-ion battery assembly, Solchenbach et al. (2014) observed the amount of intermetallic phases had strong impact on the electrical performance and contact resistance of Al–Cu welds. Instead of intermetallic phases, hot cracking is another critical issue in laser welding of dissimilar materials. Chen et al. (2011b) observed serious hot cracking developing during laser welding of Ti alloys to Ni alloys due to their significant differences of physical and thermal properties.

In order to minimise the formation of intermetallic phases and overcome differences of physical and thermal properties between welding materials, several approaches have been proposed and demonstrated through various reported work. Gao et al. (2015) selected Cu filler wire in hybrid laser-arc welding of Ti alloy and stainless steel to improve weld strength with an increase of weld homogeneity. A pure vanadium foil was introduced in laser welding of 316 L stainless steel and Ti–6Al–4V alloy by Tomashchuk et al. (2015). High weld strength was achieved after the amount of undesired intermetallic phases in welds was minimised. Two-pass laser welding was also used to anneal the welds resulting in an enhancement on its mechanical properties. Similarly, Hailat et al. (2012) placed a tin foil between the Al alloy and Cu alloy sheets in laser welding to solve the poor solubility issue. Chen et al. (2011b) offset the laser beam from the interlayer to one side of welding materials in order to achieve better weld quality.

Instead of the abovementioned methods, adopting the pulse shaping technique can be an alternative for improving weldability in laser welding of dissimilar materials. Naeem et al. (2003) described that the pulse shaping technique is a method for designing the pulse waveform of individual pulses. By properly designing the waveform of pulses delivered in laser welding, the amount of incident laser energy and the heating/cooling rates inside melting pools can be varied. Melting pool behaviours (i.e. direction of convective flow) can be totally different when different pulse profiles were applied in laser welding (Bransch et al., 1994; Ismail et al., 2012). This technique is particularly suitable for welding of materials with high thermal diffusivity and conductivity, crack-sensitive, high laser beam reflectivity and different melting points (Naeem et al., 2003). Dürr et al. (2004) used the technique to improve weldability in laser welding of refractory metals and dissimilar metals.

* Corresponding author.
E-mail address: hcchen@SIMTech.a-star.edu.sg (H.-C. Chen).

http://dx.doi.org/10.1016/j.jmatprotec.2015.12.016
0924-0136/

Table 1
Material properties of CP Ti and 304 stainless steel (Gale and Totemeier, 2004).

	CP Ti	304 stainless steel
Melting point (°C)	Max. 1665	1399–1454
Density (g/cc)	4.51	8.00
Thermal conductivity (W/m K)	16.4	138.0
Specific heat (J/g °C)	0.523	0.880
Thermal diffusivity (10^{-5} m^2/sec)	6.90	4.08
Coefficient of thermal expansion at 20 °C (10^{-5}/°C)	0.86	1.72
Hardness (Hv)	148.8	325.0
Tensile strength (MPa)	345	835

Table 2
Summary of process parameters used in this work.

	1	2	3
Peak laser power (kW)	4.5		
Pulse frequency (Hz)	7.5		
Pulse duration (ms)	1		
Pulse profiles	No PS	PS No. 1	PS No. 2
Welding speed (m/sec)	100		
Shielding gas	Argon gas		

Torkamany et al. (2014) modified the pulse profile into smaller pulse durations in laser welding of pure niobium and Ti–6Al–4V, the degree of intermixing between two welding materials was decreased resulting in less inhomogeneity in welds.

Key challenges in laser welding of CP Ti and stainless steel are caused from their great differences in thermo-physical properties, chemical compositions and low solubility. Intermetallic phases (i.e. FeTi, Fe_2Ti, $TiCr_2$ and $NiTi_2$, $Ti_5Fe_{17}Cr_5$) are likely formed during laser welding as summarised by Chen et al. (2014) and Satoh et al. (2013). Akbari Mousavi and Sartangi (2008) further indicated that FeTi and Fe_2Ti are brittle intermetallic phases. Chen et al. (2014) improved weld strength in continuous-wave laser welding of stainless steel to Ti alloys by offsetting the laser beam to the stainless steel side. The objective of this work is to study the effect of temporal pulse profiles used in laser welding of CP Ti and stainless steel. Welds obtained from different pulse profiles were evaluated in the aspect of metallurgical variations, mechanical properties and fracture modes. The melting pool behaviour, weld strength and its fracture mode were strongly depended on the pulse profiles applied in the process. Stronger welds with the complex fracture mode were achieved when a ramp-down pulse profile was selected in laser welding rather than the use of a normal rectangular pulse profile.

2. Materials and methods

Commercially pure titanium (CP Ti; Ti: 99.2 wt.%) and 304 stainless steel (Cr: 18.0–20.0, Ni: 8.0–10.5 and Fe: balance (wt.%)) sheets were laser welded by using a pulse wave Nd:YAG laser source with the wavelength of 1064 nm. The dimension of both CP Ti and 304 stainless steel sheets used in this work was 50 mm by 25 mm by 0.25^t mm. Material properties of the welding materials are summarised in Table 1. Before laser welding, the CP Ti sheet was placed on the top of the stainless steel sheet with an overlap of 10 mm, as illustrated in Fig. 1. Throughout the work, the laser beam was focused on the top surface of stainless steel sheets and positioned at the edge of the CP Ti sheet. Process parameters used in this work are tabulated in Table 2. Peak laser power, pulse frequency, pulse duration and welding speed were kept constant while three different temporal pulse profiles were used. The pulse profiles include a normal rectangular pulse profile (Fig. 2(a)) and two ramp-down pulse profiles (Fig. 2(b) and (c)). Argon gas was supplied as the shielding gas to protect the melting pool from serious oxidation during laser welding.

After laser welding, the top surface of welds was observed by optical microscopy (OM) before undergoing standard procedures for further metallurgical analysis. Cross-section of welds was measured and investigated by using both OM and scanning electron microscopy (SEM) equipped with energy dispersive spectrometer (EDS). Hardness of welds was measured by using a Vickers microhardness machine with a 50 g load for 15 s. Weld strength was evaluated by using an INSTRON 4505 universal tensile testing machine. For each welding condition, five samples were welded and tensile tested. After tensile testing, fractured surface of welds were investigated by SEM.

3. Results

3.1. General observation

Top view of welds obtained from different pulse profiles are presented in Fig. 3. When the No PS pulse profile was used, as shown in Fig. 3(a), the weld surface was less smooth and the fusion line of the weld near the stainless steel side was irregular in comparison with the welds made by using the pulse profile of PS No.1 (Fig. 3(b)) and PS No. 2 (Fig. 3(c)). For all cases shown in Fig. 3, the fusion line of the welds near the CP Ti side was straighter than that near the stainless steel side. The widest (1282 μm) and narrowest (1014 μm) welds were obtained from using of the No PS and PS No.1 pulse profiles, as shown in Fig. 3(a) and (b), respectively.

Figs. 4(a) and 5(a) are the cross section of the welds shown in Fig. 3(a) and (c), respectively. In Fig. 4(a), few cracks were observed at the location adjacent to the stainless steel side. Weld geometry in terms of area of the fusion zone, area of the fusion zone formed at the stainless steel side and depth of weld penetrated into the stainless steel side (D_p as indicated in Fig. 5(a)) are given in Fig. 6. The biggest fusion zone, around 0.20 mm^2, was obtained in laser welding with the use of the No PS pulse profile, while the smallest fusion zone, around 0.13 mm^2, was received when the PS No. 1 pulse profile was used. At the same time, areas of fusion zone formed inside the stainless steel side did not have significant differences between the uses of three different pulse profiles. Similar penetration depth (D_p) of welds were also obtained between the use of three different pulse profiles.

3.2. Microstructure of the weld

When the No PS pulse profile was used, the weld with an inhomogeneous mixing between two welding materials was observed, as shown in Fig. 4(a) and (c). In Fig. 4(a), according to the EDS results, the ivory and white colours represent the phases of Ti-rich and Fe-rich, respectively. In contrast to results obtained in Fig. 4(a) and (c), when the PS No. 2 pulse profile was used, a weld with less degree of intermixing between two welding materials was observed in Fig. 5(a) and (c). In Fig. 5(a), only small Fe-rich (white colour) and Ti-rich (ivory colour) islands were observed in the welds. Average hardness of these Fe-rich and Ti-rich islands were 429 Hv and 284 Hv, respectively. In Fig. 4(b), the weld with clear eddy flows was presented. It tells that two welding materials were drastically intermixed in the melting pool during laser welding. Dendrite structures were observed in Zone 1 of the weld, as shown in Fig. 4(d). In Fig. 4(f), a dendritic zone with same microstructure orientation was found in area next to the CP Ti substrate.

Microstructure of the weld made by using the PS No. 2 pulse profile is displayed in Fig. 5(c)–(f). Compared to the microstructure shown in Fig. 4(b), several individual islands were formed within the weld as shown in in Fig. 5(c). Similar dendritic structures were

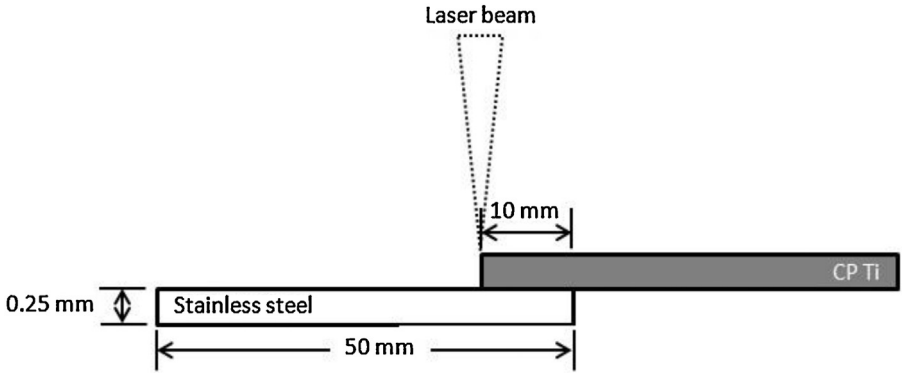

Fig. 1. Schematic of the experimental setup in this work.

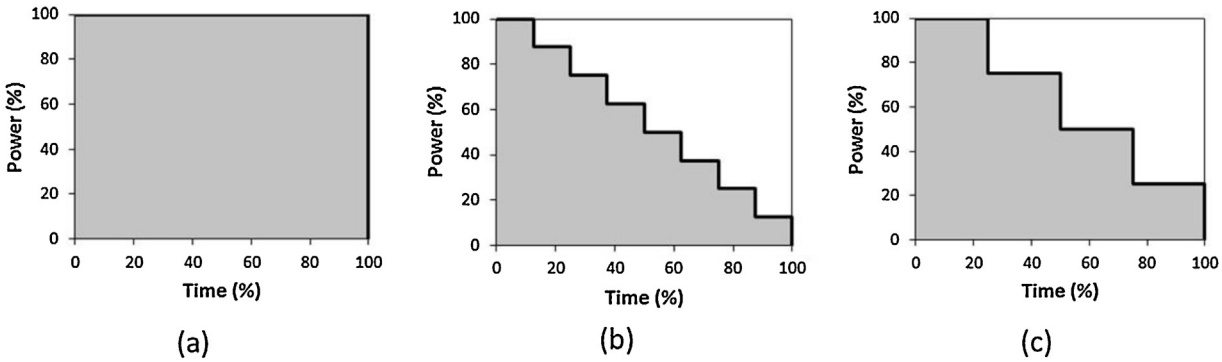

Fig. 2. Illustration of the pulse profiles used in this work: (a) No PS; (b) PS No. 1; (c) PS No. 2.

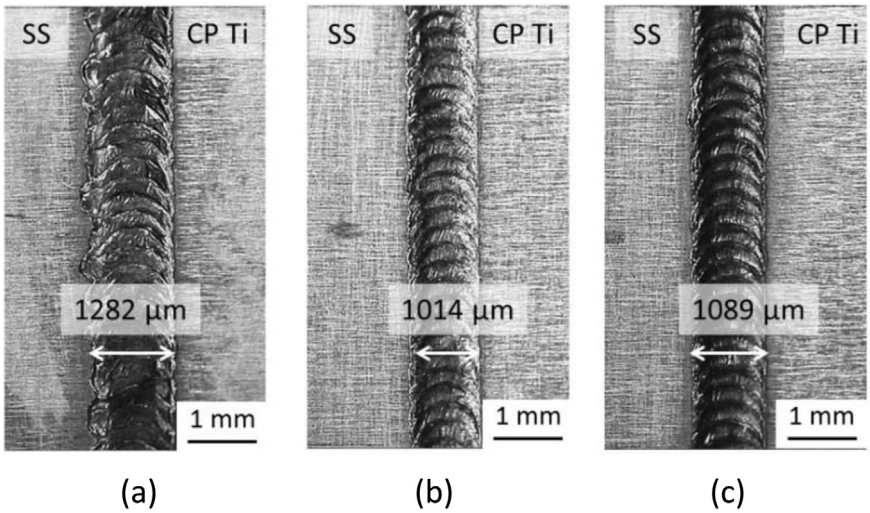

Fig. 3. Top view of welds in laser welding of CP Ti and stainless steel with different pulse profiles: (a) No PS; (b) PS No. 1; (c) PS No. 2. ("SS" means stainless steel).

observed at the near centre area (Zone 5) of the weld in Fig. 5(d). At the lower part of the weld, two regions (with black and white colour) were clearly presented in Fig. 5(e). At the location next to the un-welded CP Ti substrate, in Fig. 5(f), a narrower dendrite zone was observed in comparison with that shown in Fig. 4(f).

3.3. Chemical compositions of the weld

SEM EDS line scanning results along the Line-A (in Fig. 4(a)) and Line-B (Fig. 5(a)) of the welds are displayed in Figs. 4(b) and 5(b), respectively. Although Ti was the major element in both welds, drastic changes of Ti and Fe elements were detected in the weld, as shown in Fig. 4(b). Fe became the major element after the scanning line entered into the stainless steel side. Although Ti remained as the major element within the weld, In Fig. 5(b), the profile was relatively stable. Similar result was obtained on the Fe element. After the scanning line entered into the stainless steel side, the amount of Ti element immediately reduced and became the minority. At the same time, both Fe and Cr elements drastically increased and became the first and second major elements. In Fig. 4(e), EDS line-scanning results show dramatic changes of Ti and Fe elements across the cracks. In comparison with the 33 area% of Ti contented in the weld (Fig. 4(b)), a higher area percentage of Ti (57 area%) was found in the weld of Fig. 5(b).

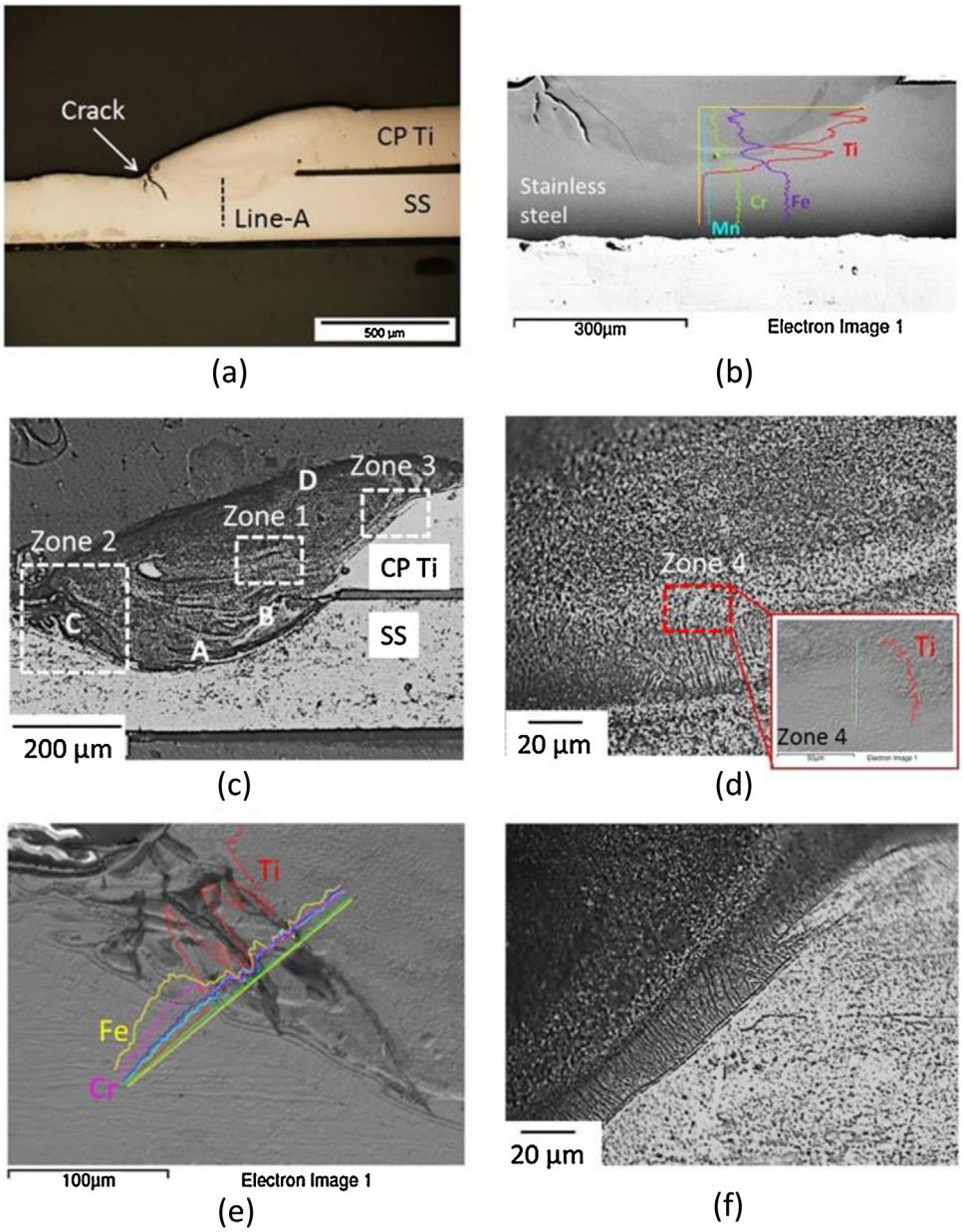

Fig. 4. Laser welding of CP Ti and stainless steel with the No PS pulse profile: (a) cross-section of the weld; (b) SEM EDS line-scanning results at the lower part of the weld; (c) microstructure of the cross-sectional weld; (d) high resolution image at Zone 1 of (c); (e) SEM EDS line-scanning results at Zone 2 of (c); (f) High resolution image at Zone 3 of (c).

Table 3
EDS and hardness results at Points A–H highlighted in Figs. 4 and 5.

Point	Chemical composition (at%)				Hardness(Hv)	Phase
Fe	Ti	Cr	Ni			
A	41.53	25.96	11.42	4.55	650.9	Fe_2Ti
B	2.52	88.53	0.65	–	363.5	Ti-rich
C	58.46	18.34	16.68	6.52	650.3	Fe_2Ti
D	43.52	42.22	9.36	4.62	521.0	FeTi
E	39.92	50.64	5.54	3.59	580.7	FeTi
F	33.72	58.59	4.43	3.02	590.5	FeTi
G	10.21	86.76	2.72	–	283.9	Ti-rich
H	53.83	23.27	15.98	6.54	601.0	Fe_2Ti

EDS and hardness results of Points A–H highlighted in Figs. 4 and 5 are tabulated in Table 3. Each of them has different chemical compositions and hardness values. For instance, the hardest point was found at Point A which was likely to be the brittle Fe_2Ti intermetallic phases. In overall, brittle phases (Fe_2Ti) are easily formed at the bottom part of welds adjacent to the stainless steel substrate, such as Points A, C and H. The FeTi phase was easily formed in the upper part of welds (i.e. Points D–F).

3.4. Mechanical properties of the weld

Fig. 7 gives hardness distributions in the welds. As illustrated in Fig. 7, the hardness values were measured starting from the fusion line next to the un-welded CP Ti substrate and the half height of the welds. The distance between each measured point was kept at 0.05 mm along the horizontal line. In overall, a relatively lower hardness distribution was obtained in the weld which was made by using the PS No. 2 pulse profile. The hardness values obtained from the welds made by using the No PS and PS No. 1 pulse profiles were slightly random. All hardness values were higher than the average

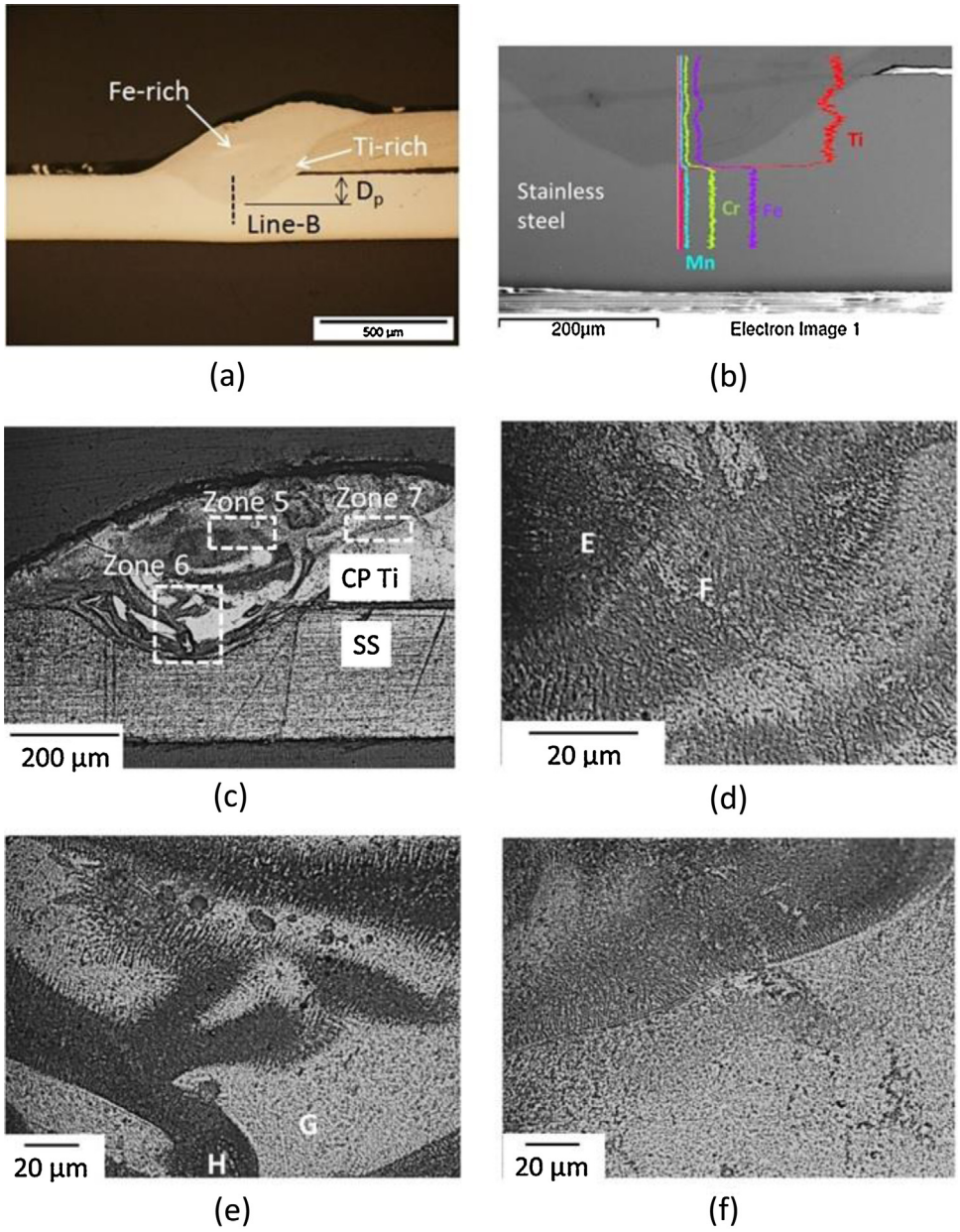

Fig. 5. Laser welding of CP Ti and stainless steel with the PS No. 2 pulse profile: (a) Cross-section of the weld; (b) SEM EDS line-scanning results at the lower part of the weld; (c) Microstructure of the cross-sectional weld; (d) High resolution image at Zone 5 of (c); (e) SEM EDS line-scanning results at Zone 6 of (c); (f) High resolution image at Zone 7 of (c).

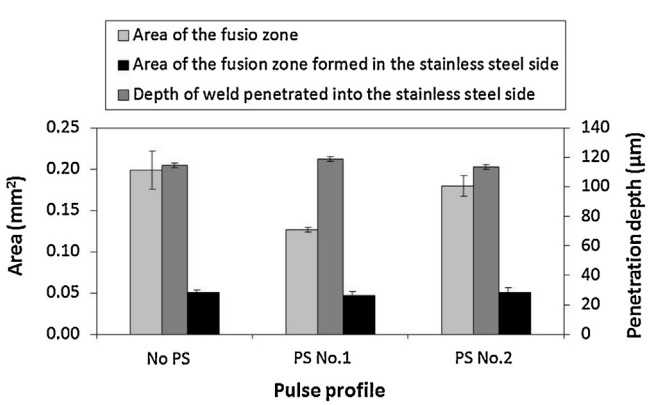

Fig. 6. Relationship between weld geometry and the pulse profiles used in laser welding.

hardness of the as-received CP TI (Hv 150) and stainless steel (Hv 325) sheets.

Results of the ultimate tensile strength of welds are given in Fig. 8. The lowest weld strength, 65 MPa, was received from the welds made by using the No PS pulse profile. The strongest weld, around 70% of the as-received CP Ti sheet, was obtained with the use of the PS No. 1 pulse profile. Although similar values were received from the welds generated between the use of PS No. 1 and PS No. 2 pulse profiles, the joint strength with a higher standard deviation was observed from the samples made by the PS No. 1 pulse profile.

3.5. Fracture analysis of the weld

Fig. 9(a) is a top view image of the fractured weld which was obtained by using the No PS pulse profile. After tensile testing, the weld broke at the area near the CP Ti side. Its broken line was almost

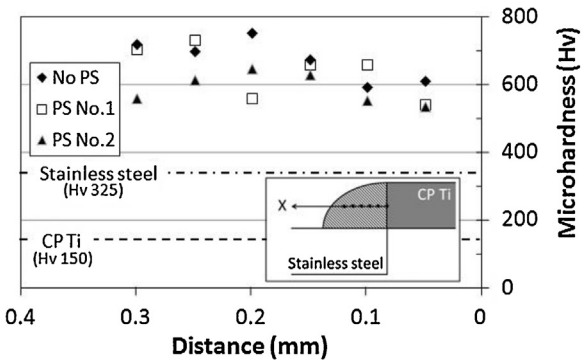

Fig. 7. Hardness distributions in the welds obtained from the use of different pulse profiles.

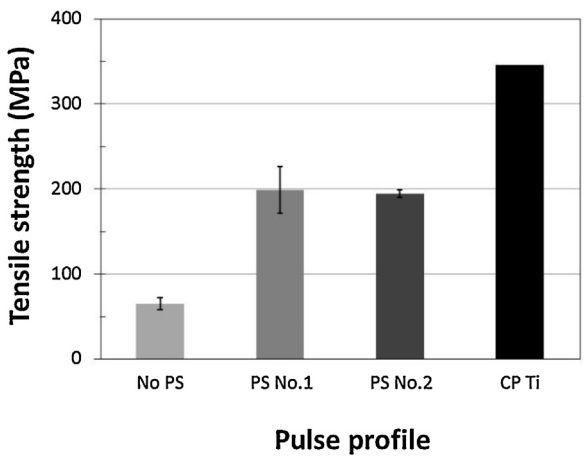

Fig. 8. Ultimate tensile strength of welds obtained from laser welding with different pulse profiles. (Strength of CP Ti was obtained from the as-received CP Ti sheets).

parallel to the edge of the weld on the CP Ti side. A high magnification image from the fractured stainless steel side is shown in Fig. 9(b). A clear crack propagated across several welded spots is observed. At the same time, a brittle fracture mode is obtained from the CP Ti side, as shown in Fig. 10(a). Large areas with significant topographical changes were observed.

A top view of the fracture weld obtained from the use of PS No. 2 pulse profile is shown in Fig. 9(c). Similarly, the broken line of the weld was closer to the CP Ti side. Two different types of the fractured zones, indicated as PS No. 2-1 and PS No. 2-2 in Fig. 9(c), were observed on the fractured weld. The first type of the fractured zone was shown in Fig. 9(d). The broken line was parallel to the edge of the weld on the CP Ti side. For the second type of the fractured zone, the partial weld was delaminated from the stainless steel side, as indicated as the zone of PS No. 2-2 in Fig. 9(c). Its SEM high magnification image is shown in Fig. 9(e). The cleavage morphology was observed from the fractured surface on the stainless steel side of the fractured weld. In Fig. 10(b), a complex fracture mode is observed from the fractured CP Ti side.

4. Discussion

In pulsed laser welding, key processing parameters include peak laser power, pulse frequency, pulse duration, welding speed and pulse profile. The value of peak power applied in laser welding mainly determines the penetration depth of welds (Kim et al., 2002), while size of fusion and heat affected zones of welds are related to the amount of average laser energy transferred into welding materials. The value of average laser energy can be considered as a function of pulse frequency, pulse duration, weld speed, pulse profile. . .etc. Because the peak power were kept constant in this study, similar penetration depths of weld were obtained between the use of three different pulse profiles as depicted in Fig. 6. There was an interesting relationship between weld dimension and the average laser energy applied in the process. Since pulse frequency, pulse duration and weld speed were all kept constant, the amount of average laser energy was directly determined by the pulse profile used. In comparison with using a rectangular pulse profile (Fig. 2(a)), less laser energy will be applied onto welding materials when a ramp-down pulse profile (Fig. 2(b) or (c)) is used in laser welding. That is due to the laser energy is gradually reduced over time within a pulse. When less laser energy is interacted with welding materials, a smaller weld size will be created. Hence, as summarised in Fig. 6, the smallest weld was obtained when the PS No. 1 pulse profile was used.

For dissimilar materials welding, main challenges are resulted from different material properties between welding materials which will seriously affect their weldability. In this work, as reported in Table 1, thermal conductivity of stainless steel (138 W/m K) is approximately nine times higher than that of CP Ti (16.4 W/m K). Due to their great differences, laser energy absorbed by the CP Ti sheet (the top welding material) will easily be accumulated inside the CP Ti side rather than transferred into the stainless steel side (the bottom welding material). Heat accumulation will become more significant when high laser energy is applied. With these reasons, as shown in Fig. 6, a bigger weld was obtained from the use of a No PS pulse profile. Besides, the melting area within the CP Ti side was always bigger than the area within the stainless steel side. Since the penetration depth of welds is determined by the value of peak power applied, the melting area in the stainless steel side will be formed at the initial stage of each pulse (Kim et al., 2002). Hence, the weld penetration depth and the melting area inside the stainless steel side did not have obvious changes between the uses of three different pulse profiles.

When both CP Ti and stainless steel sheets were melted, the two materials will intermix with each other within the melting pool. The degree of intermixing is strongly determined by the convective flow (Marangoni effect) which is driven by the spatial gradient of surface tension at the melt pool surface due to its local temperature variation (Wei et al., 2015; Mills et al., 1998). Strength of convective flow is affected by the laser power energy applied in laser welding (Russo et al., 1990). In comparison with welds made by using a ramp-down pulse profile (Fig. 5(c)), weld microstructure with obvious eddies (Fig. 4(c)) was observed when a rectangular pulse profile (No PS pulse profile) was used. It was due to higher laser energy was applied for the welding process. The inhomogeneous intermixing between the two welding materials caused an increasing amount of intermetallic phases in welds. Most of them are brittle intermetallic phases (i.e. FeTi and Fe_2Ti), as indicated in Table 3. In contrast, the weld which was made up of several individual islands and contented a higher area percentage of Ti was observed when a ramp-down pulse profile was used as in Fig. 5(c). The gradual decrease of laser energy supplied by a ramp-down pulse profile contributed to less convective flow and minimised the degree of intermixing between two welding materials in welds (Russo et al., 1990). That was resulted from the lower thermal gradient generated in the melting pool. The size of dendritic zones shown in Figs. 4 (f) and 5 (f) also show evidences that a lower thermal gradient was developing inside the melting pool when a ramp-down pulse profile was used. Although brittle intermetallic phases were observed, welds with better homogeneous were received. As these, stronger welds with the complex fracture mode were achieved by using a ramp-down pulse profile rather than using a rectangular pulse profile.

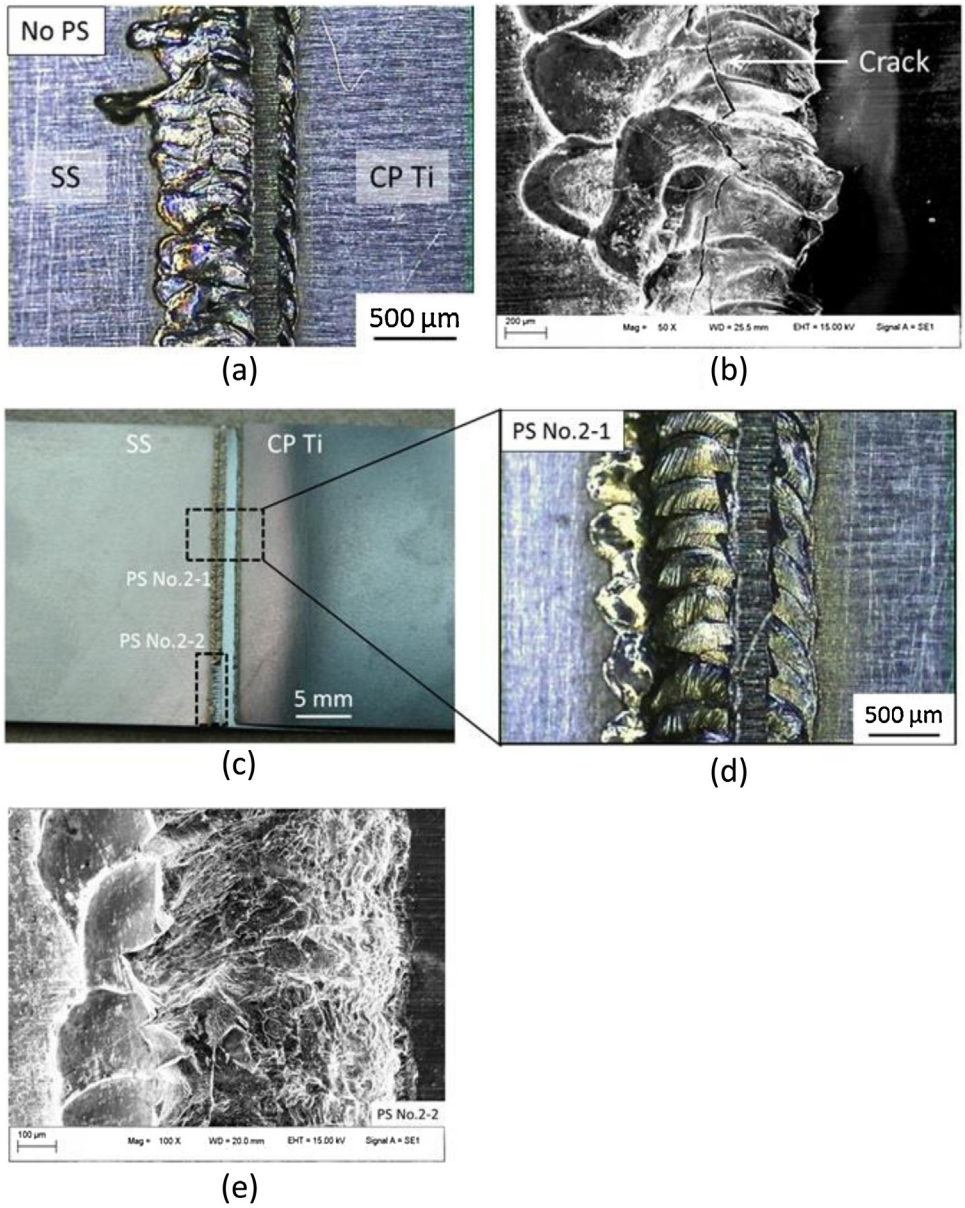

Fig. 9. Top view of welds after tensile tests: (a) the fractured weld obtained from the use of the No PS pulse profile; (b) a high resolution image on the stainless steel side shown in (a); (c) the fractured weld obtained from the use of the PS No. 2 pulse profile; (d) a high resolution image of the fractured weld at the PS No. 2-1 zone as indicated in (c); (e) a SEM high magnification image from the PS No. 2-2 zone as indicated in (c).

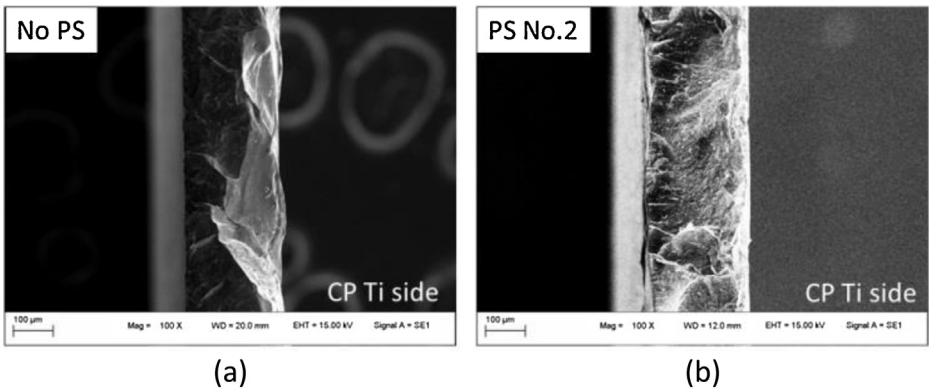

Fig. 10. Fractured surface of the welds obtained from laser welding with the use of different pulse profiles: (a) No PS; (b) PS No. 2.

5. Conclusions

The effect of temporal pulse profiles used in laser welding of CP Ti and stainless steel was investigated in this study. Results show that weld quality in terms of weld appearance, weld geometry, the formation of intermetallic phases, mechanical properties of welds and the fracture mechanism strongly depended on the pulse profiles used in laser welding. The observations and findings are summarised as below,

- The welds with better appearance were obtained by using the PS No. 2 pulse profile, while the welds with irregular appearance were obtained by using the No PS pulse profile.
- With the use of the PS No. 1 or PS No. 2 pulse profile, the degree of intermixing between two welding materials in welds can be effectively restricted resulting in less formation of intermetallic phases. Stronger weld was achievable in comparison with the use of No PS pulse profile.
- The highest weld strength obtained from the use of PS No. 1 pulse profiles achieved approximately 70% of the strength of the as-received CP Ti sheets.
- The fracture mode of the welds transformed from the brittle mode to the complex mode when the pulse profile used in laser welding was changed from the No PS pulse profile to the PS No. 1 or PS No. 2 pulse profile.
- In this study, results did not show obvious difference between the use of two ramp-down pulse profiles, PS No. 1 and PS No. 2. More investigations must be conducted as the future work.

References

Akbari Mousavi, S.A.A., Sartangi, P.F., 2008. Effect of post-weld heat treatment on the interface microstructure of explosively welded titanium–stainless steel composite. Mater. Sci. Eng. 494, 329–336.

Bransch, H.N., Weckman, D.C., Kerr, H.W., 1994. Effects of pulse shaping on Nd:YAG spot welds in austenitic stainless steel. Weld. Res. Suppl., 141-s–151-s.

Chen, H.-C., Pinkerton, A.J., Li, L., Liu, Z., Mistry, A.T., 2011a. Gap-free fibre laser welding of Zn-coated steel on Al alloy for light-weight automotive applications. Mater. Des. 32, 495–504.

Chen, H.C., Pinkerton, A.J., Li, L., 2011b. Fibre laser welding of dissimilar alloys of Ti-6Al-4 V and Inconel 718 for aerospace applications. Int. J. Adv. Manuf. Technol. 52, 977–987.

Chen, S., Zhang, M., Huang, J., Cui, C., Zhang, H., Zhao, X., 2014. Microstructures and mechanical property of laser butt welding of titanium alloy to stainless steel. Materi. Des. 53, 504–511.

Dürr, U., Holtz, R., Jokiel, M., Liebers, R., Lavoie, D., 2004. Advanced micro-welding strategies with pulsed Nd:YAG lasers. In: ICALEO 2004—23rd International Congress on Applications of Laser and Electro-Optics, Congress Proceedings, United States.

Gale, W.F., Totemeier, T.C., 2004. Smithells Metals Reference Book, 8th ed. Elsevier.

Gao, M., Chen, C., Wang, L., Wang, Z., Zeng, X., 2015. Laser-arc hybrid welding of dissimilar titanium alloy and stainless steel using copper wire. Metall. Mate. Trans. A 46, 2007–2020.

Hailat, M.M., Mian, A., Chaudhury, Z.A., Newaz, G., Patwa, R., Herfurth, H.J., 2012. Laser micro-welding of aluminum and copper with and without tin foil alloy. Microsyst. Technol. 18, 103–112.

Mills, K.C., Keene, B.J., Brooks, R.F., Shirali, A., et al., 1998. Marangoni effects in welding. Philos. Trans. R. Soc. A-Math. Phys. Eng. Sci. 356, 911–925, ISSN: 1364-503X.

Ismail, M.I.S., Okamoto, Y., Okada, A., Uno, Y., Ueoka, K., 2012. Direct micro-joining of flexible printed circuit and metal electrode by pulsed Nd:YAG laser. Int. J. Precis. Eng. Manuf. 13, 321–329.

Kim, B.-C., Kim, T.-H., Kim, K.-B., Kim, J.-S., Lee, H.-Y., 2002. Investigation on the effect of laser pulse shape during Nd:YAG laser microwelding of thin Al sheet by numerical simulation. Metall. Mater. Trans. A 33, 1449–1459.

Meco, S., Pardal, G., Ganguly, S., Williams, S., McPherson, N., 2015. Application of laser in seam welding of dissimilar steel to aluminium joints for thick structural components. Opt. Laser. Eng. 67, 22–30.

Naeem, M., Jessett, R., Kugler, T., 2003. The influence of pulse shaping on welding. In: The 22nd International Congress on Applications of Lasers & Electro Optics, Jacksonville, FL.

Russo, A., Akau, R., Jellison, J., 1990. Thermocapillary flow in pulsed laser beam weld pools. Weld. J. 69, 23–29.

Satoh, G., Yao, Y.L., Qiu, C., 2013. Strength and microstructure of laser fusion-welded Ti–SS dissimilar material pair. Int. J. Adv. Manuf. Technol. 66, 469–479.

Solchenbach, T., Plapper, P., Cai, W., 2014. Electrical performance of laser braze-welded aluminum–copper interconnects. J. Manuf. Processes 16, 183–189.

Tomashchuk, I., Grevey, D., Sallamand, P., 2015. Dissimilar laser welding of AISI 316L stainless steel to Ti6–Al4–6V alloy via pure vanadium interlayer. Mater. Sci. Eng. 622, 37–45.

Torkamany, M.J., Malek Ghaini, F., Poursalehi, R., 2014. Dissimilar pulsed Nd:YAG laser welding of pure niobium to Ti–6Al–4V. Mater. Des. 53, 915–920.

Wei, H.L., Mazumder, J., DebRoy, T., 2015. Evolution of solidification texture during additive manufacturing. Sci. Rep. 5, 16446.